Science Talks 3 (2022) 100054

Contents lists available at ScienceDirect

Science Talks

journal homepage: www.elsevier.es/sctalk

Control of purely-elastic instabilities in cross-slot geometries

Mahdi Davoodi [a,*,1], Gemma Houston [b], Allysson Domingues [a], Jenna Downie [b], David Dennis [a], Mónica S.N. Oliveira [b], Robert J. Poole [a]

[a] School of Engineering, University of Liverpool, Liverpool, L69 3GH, UK
[b] James Weir Fluids Laboratory, Department of Mechanical and Aerospace Engineering, University of Strathclyde, Glasgow G1 1XJ, UK

ARTICLE INFO

Keywords:
Microfluidics
Viscoelasticity
Instability control

ABSTRACT

The cross-slot stagnation point flow is one of the benchmark problems in fluid mechanics as it allows large strains to develop and can therefore be used in extensional rheometry. In such a flow, for purely-elastic cases in creeping flow regimes, elasticity can break symmetry which is perhaps an unwanted phenomenon if used as a rheometer and will limit the maximum deformation rate in which these tests can be performed, or beneficial once used as mixing device. Here, this instability will be investigated in more detail using a combination of numerical, experimental and analytical analysis and a series of methods will be proposed that can potentially be used to delay and control the start point of the instability.

The first part of this presentation focuses on the effect of elongational dominated flow on the onset criteria of symmetry-breaking purely-elastic instability in the cross-slot geometry by applying a fundamental change on the kinematics of the flowfield in this region. Here, the standard geometry is modified by adding a cylinder at the geometric centre and replacing the free stagnation point by pinned stagnation points at the cylinder walls.

Next, two-phase flows of Newtonian and/or viscoelastic fluids in a "cross-slot" geometry will be investigated in the creeping-flow limit. In this part, the effect of injecting two fluids with different elastic properties from each inlet arm, and effects of interfacial tension and the viscosity ratio of these flow streams will be investigated.

Videos to this article can be found online at https://doi.org/10.1016/j.sctalk.2022.100054.

* Corresponding author.
E-mail address: MDavoodi@slb.com (M. Davoodi).
[1] Schlumberger Cambridge Research, UK.

http://dx.doi.org/10.1016/j.sctalk.2022.100054
Received 10 June 2022; Accepted 21 June 2022

Figures and tables

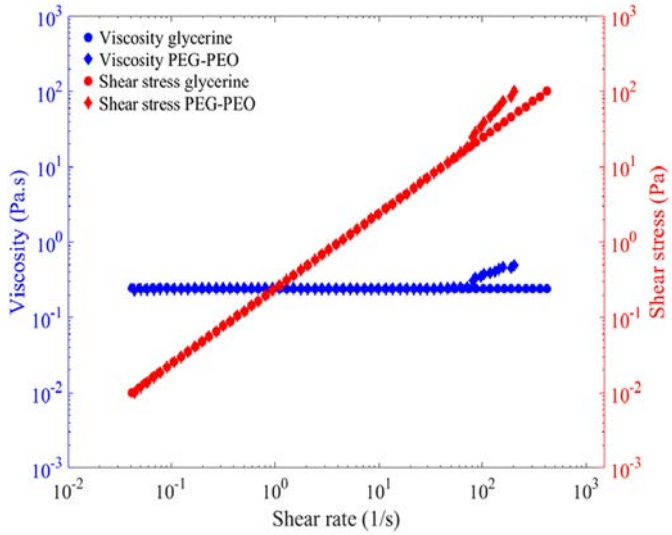

Fig. 1. The experimental shear viscosity data of Boger viscoelastic and Newtonian fluids.

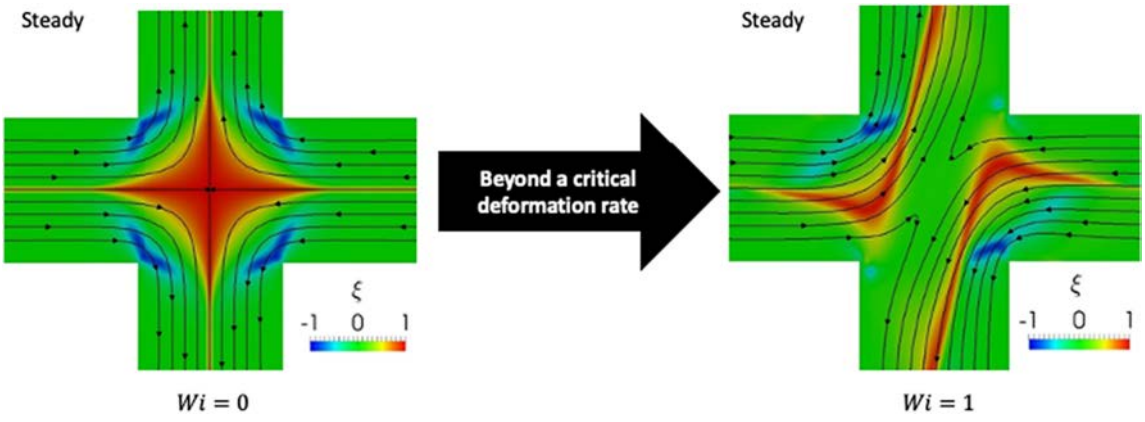

Fig. 2. Effect of viscoelasticity on the 2-D steady symmetry-breaking instability and the flow type parameter.

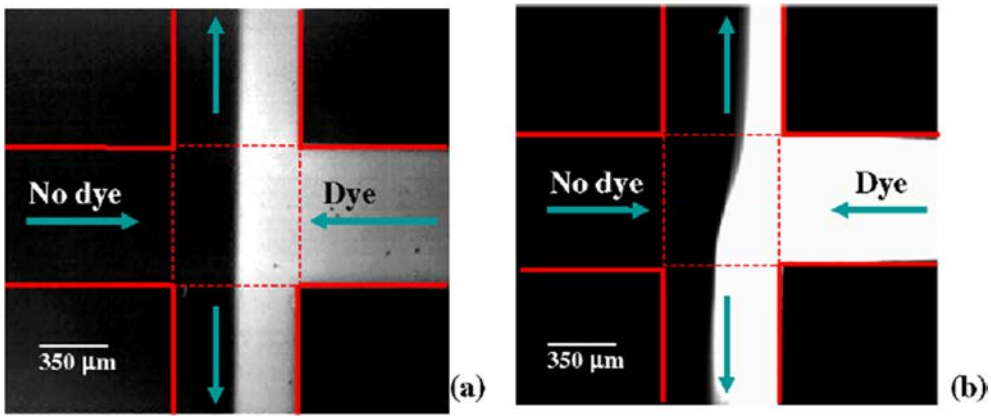

Fig. 3. Dye advection patterns for a cross-channel flow with two inputs and two outputs for (a) Newtonian fluid, and (b) PAA flexible polymer solution. Figure taken from [1].

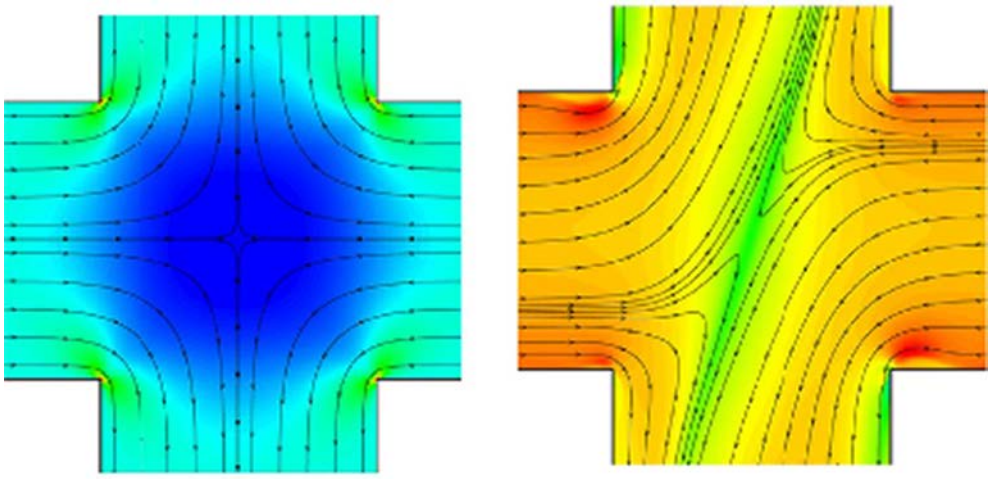

Fig. 4. Streamline patterns superimposed onto contour plots of $(\tau_{xx} - \tau_{yy})/(\eta U/D)$ for (left) Newtonian fluid, (right) viscoelastic fluids. Figure taken from [2].

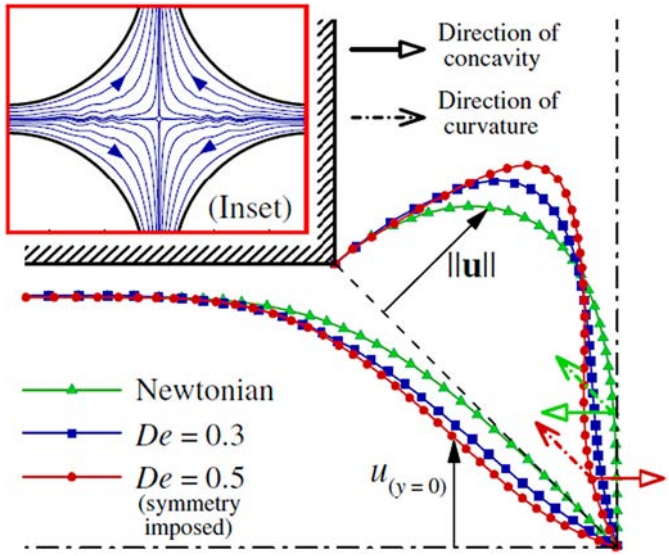

Fig. 5. Velocity profiles along horizontal centerline and along $\frac{y}{x} = -1$line (i.e., cross-slot diagonal) for $Re = 0$ and $De = 0.3$, and 0.5 (symmetry-imposed). Inset: A snapshot of the streamlines for a transient simulation for a rounded corner case ($De = 2$). Figure taken from [2].

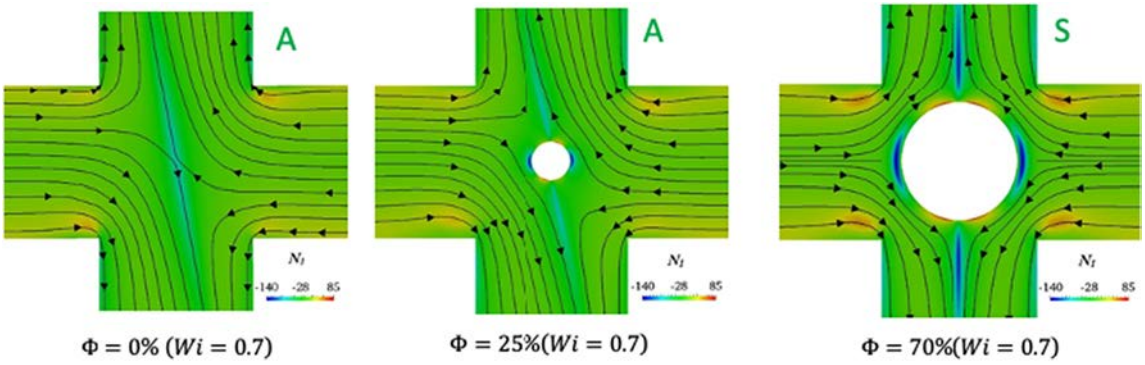

Fig. 6. Effect of geometry modification on streamlines superimposed onto contour plots of non-dimensional first normal-stress difference. Figure taken from [3].

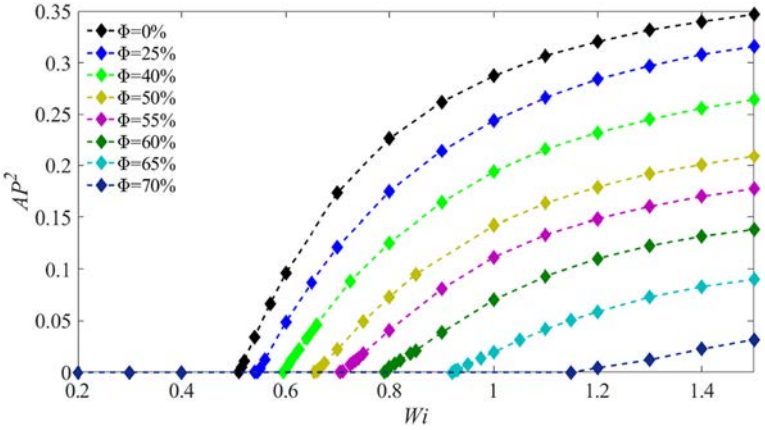

Fig. 7. Effect of Weissenberg number on the symmetry-breaking Instability and different blockage ratios. Figure taken from [3].

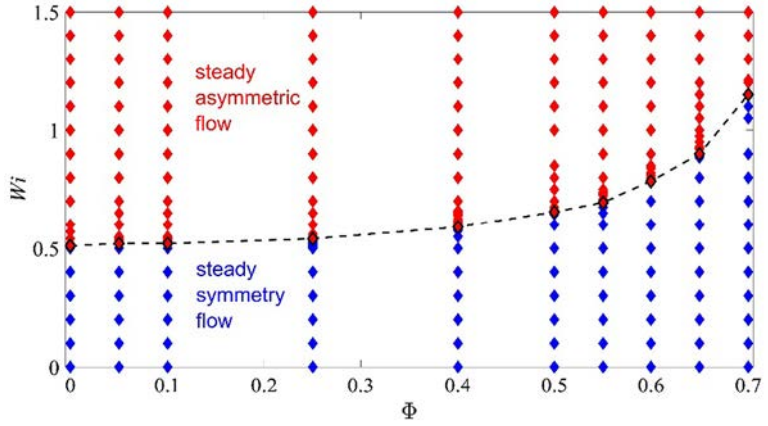

Fig. 8. Boundary between the symmetric and asymmetric flow for different *Wi* and blockage ratio. Figure taken from [3].

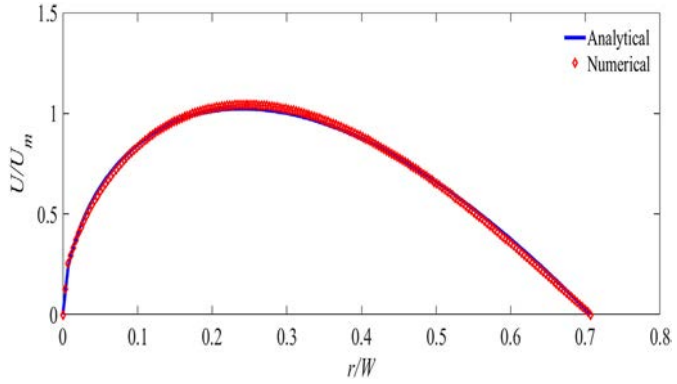

Fig. 9. Velocity distribution along the radial direction at $\theta = 0$ for both the analytical and numerical simulations for standard cross-slot geometry, Newtonian fluid. Figure taken from [3].

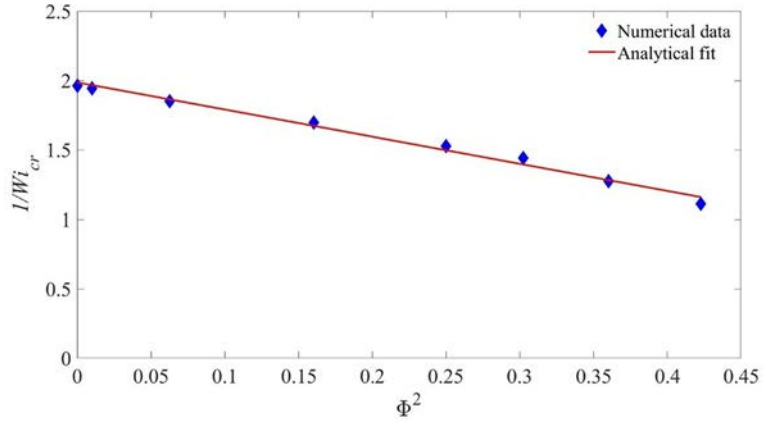

Fig. 10. Variation of critical values of Weissenberg number against the blockage ratio parameter. Figure taken from [3].

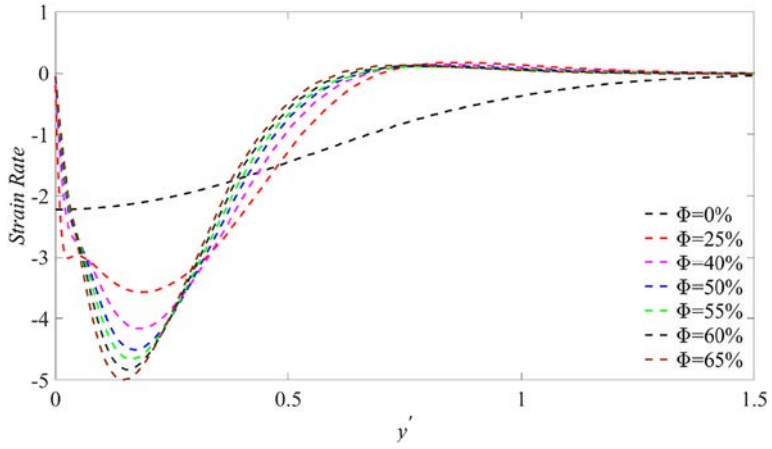

Fig. 11. Effect of blockage ratio parameter on the flow strain rate before the start of instability for $\alpha = 0.02$ and $\beta = 1/9$ along horizontal line. Figure taken from [3].

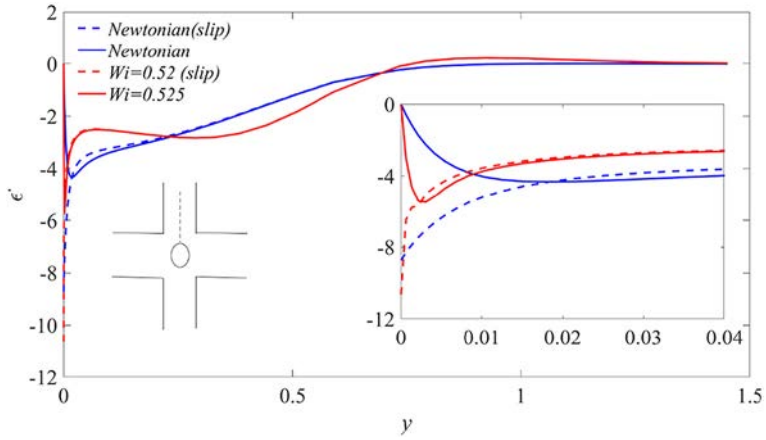

Fig. 12. Effect of slip boundary condition at the cylinder on flow strain rate along (a) horizontal line. Figure taken from [3].

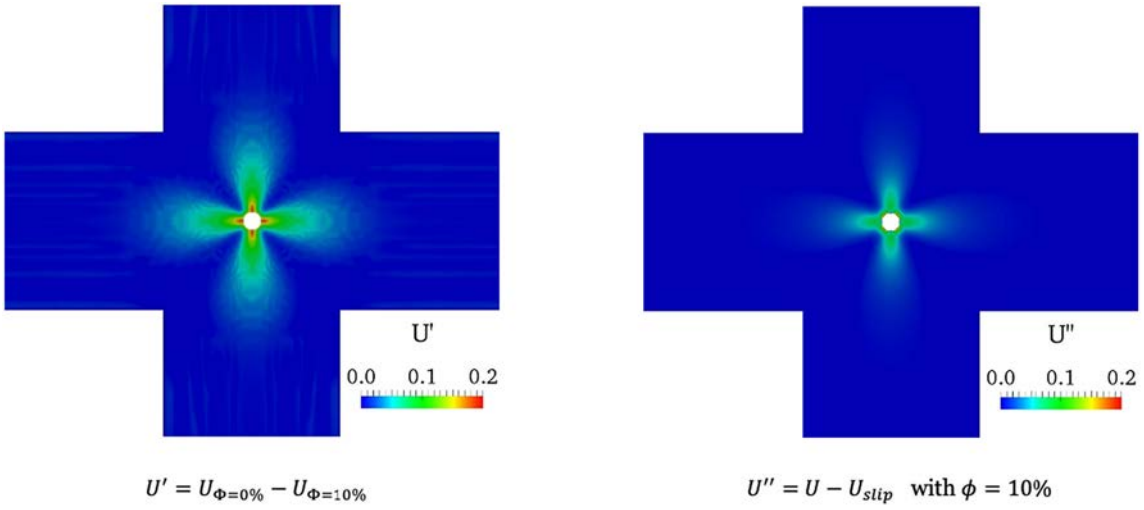

Fig. 13. Effect of (a) geometry modification and (b) slip boundary condition on the magnitude of the velocity field for creeping Newtonian fluid flows. Figure taken from [3].

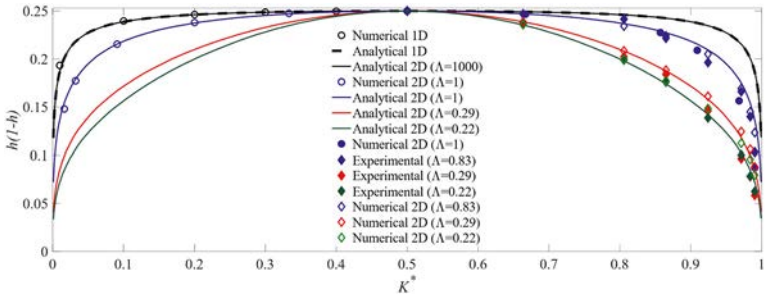

Fig. 14. Variation of the height of the interface between two fluids with viscosity ratio for Newtonian fluids. Figure taken from [4].

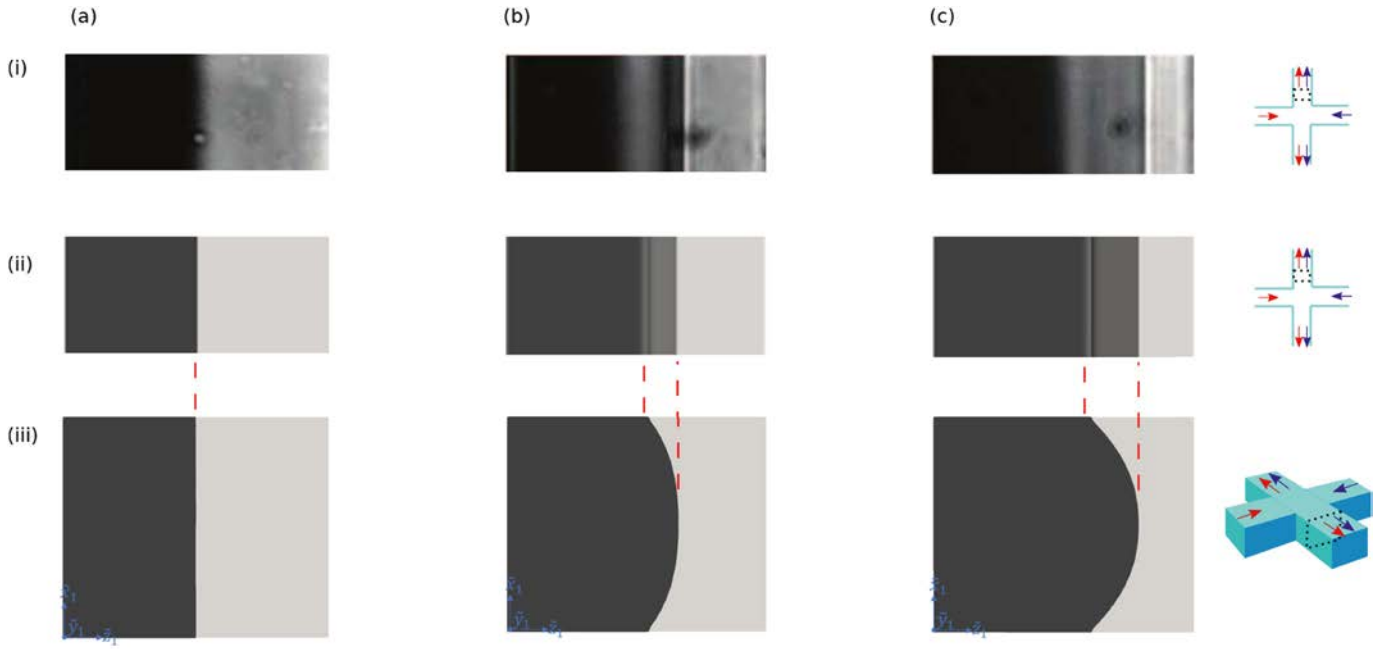

Fig. 15. Visualization of the interface between two Newtonian fluids in the fully developed region of the outlet arm with $Ca \to \infty$ and viscosity ratios (a) $K = 1$, (b) $K = 0.16$, (c) $K = 0.03$ (where the fluid shown in dark grey is the most viscous one) using $\Lambda = 0.83$ (i) in the experiment and (ii–iii) in numerical simulations. Figures (i) and (ii) are presented in (x, y) plane centred at $z = 0$ for $1.5 < y < 2$ while (iii) show a cross-sectional view of the channel ((x,z) plane) at $y = 1$. Figure taken from [4].

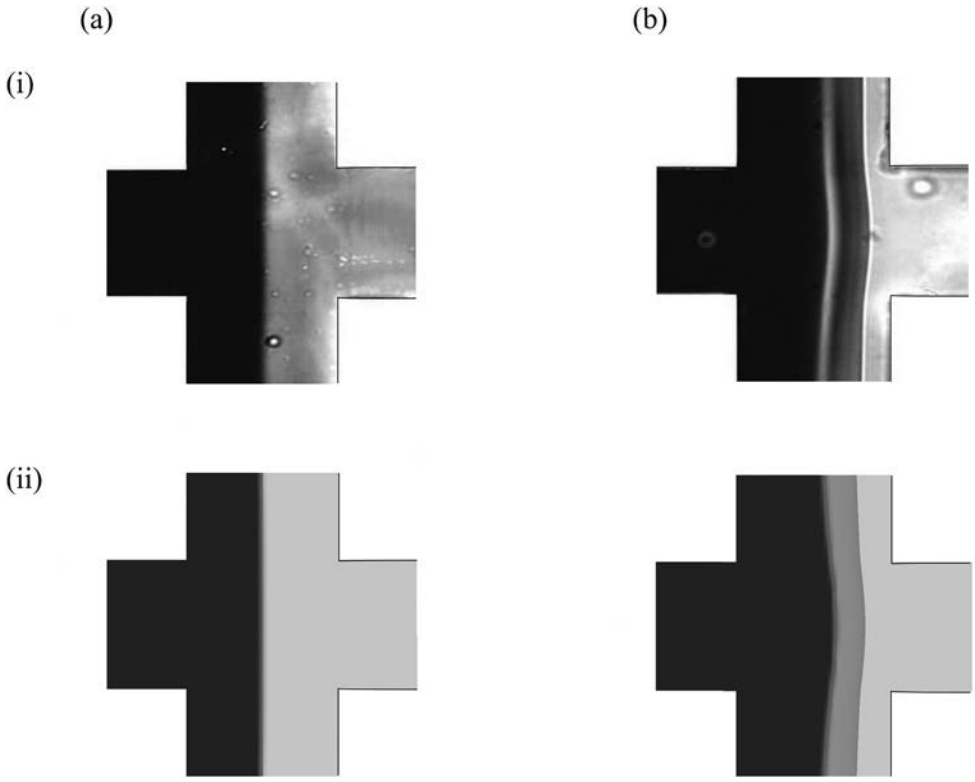

Fig. 16. Effect of viscosity ratio with $Ca = \infty$ and (a) $K = 1$, (b) $K = 0.03$ for $\Lambda = 0.83$ in (i) the experiment and (ii) in numerical simulations, where the most viscous fluid (fluid-1) is on the left-hand side. Figure taken from [4].

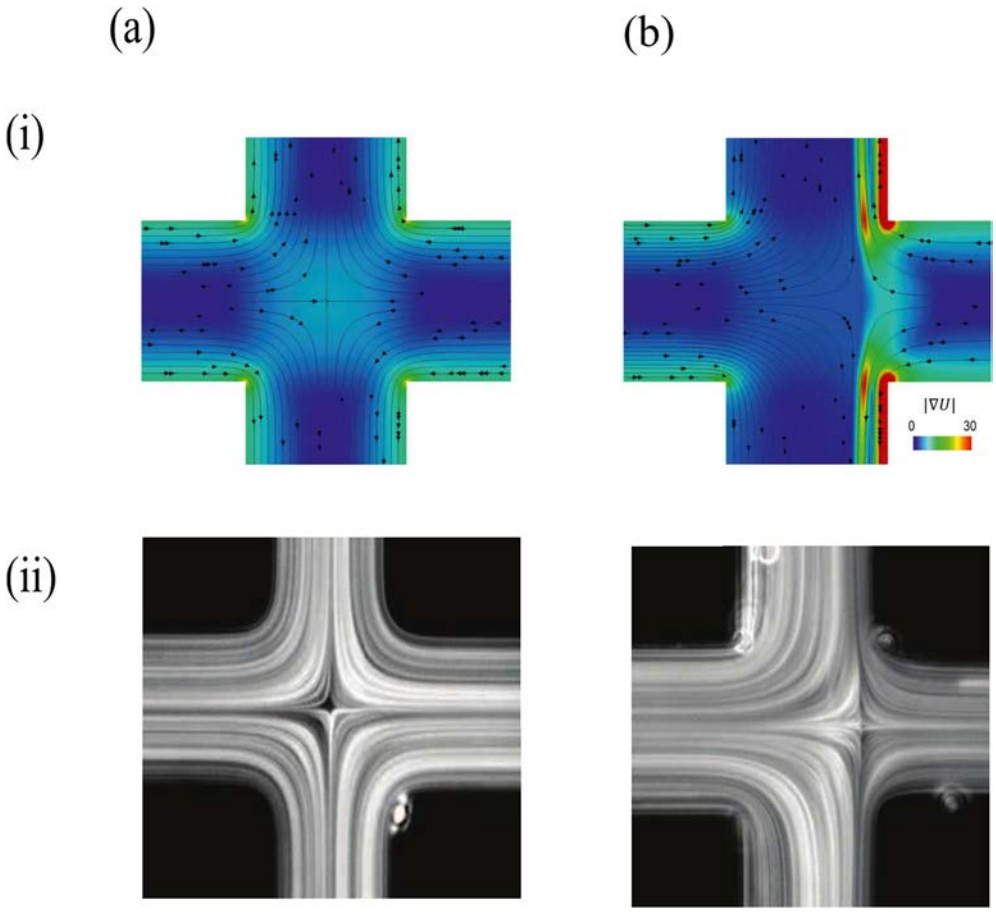

Fig. 17. Streamlines obtained using (i) numerical method superimposed on the magnitude of the non-dimensional velocity gradient with $\Lambda = 0.83$ and $Ca = \infty$ and (ii) experimental results with $\Lambda = 0.83$ for (a) $K = 1$, (b) $K = 0.16$, where the most viscous fluid enters through inlet-1 (on the left-hand side). Figure taken from [4].

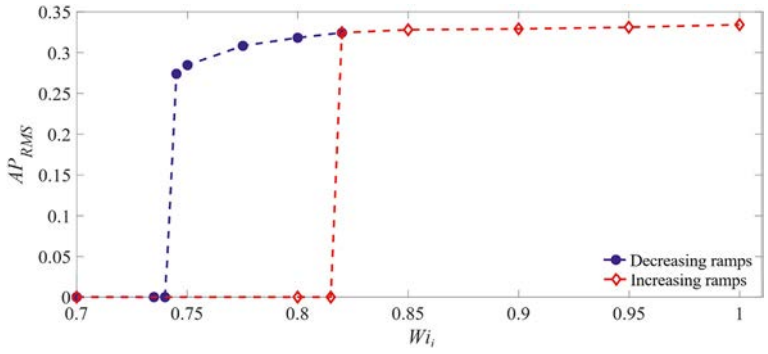

Fig. 18. The variation of r.m.s. of the asymmetry parameter for the time-dependent symmetry-breaking instability with $K = 0.001$ and $Ca = 0.005$ using an increasing Wi_i ramp (open) and decreasing ramp (closed symbols). Figure taken from [4].

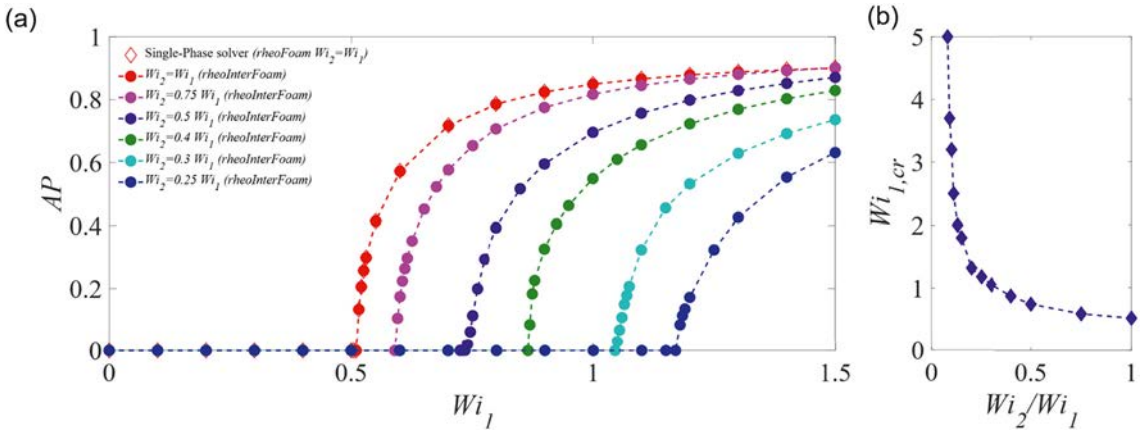

Fig. 19. (a) The stability diagram for symmetry-breaking instability and (b) the variation of critical Weissenberg number with the ratio of Weissenberg numbers for two-phase flow problems with $Ca = \infty$ and $K = 1$. Figure taken from [4].

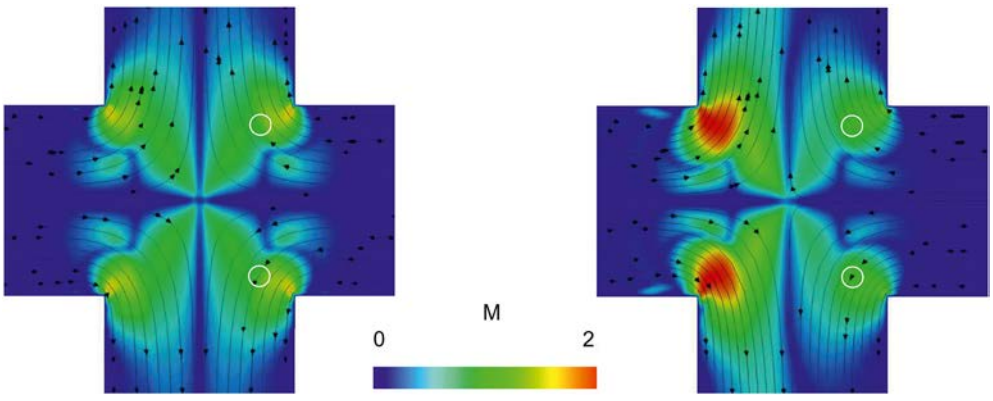

Fig. 20. The local distribution of the M parameter before the onset of the instability at (left) $Wi_1 = 0.51$ and (right) $Wi_1 = 1.18$ for (left) $Wi_2/Wi_1 = 1$, and (right) $Wi_2/Wi_1 = 0.25$ with $Ca = \infty$ and $K = 1$. The white circles indicate the location where M reaches a critical value of ≈ 1 in fluid 2. Figure taken from [4].

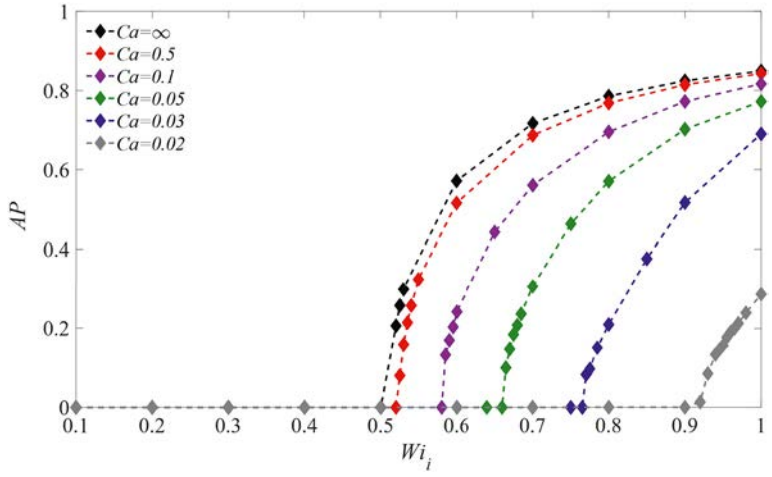

Fig. 21. Effect of Wi_i with $i = \{1,2\}$ on the steady symmetry-breaking instability for $K = 1$ and different capillary numbers. Figure taken from [4].

Acknowledgments

- Rob Poole
- Morton Denn
- Andrew Clarke
- Gareth McKinley
- Manuel Alves

Declaration of interests

The authors declare that they have no known competing financial interests or personal relationships that could have appeared to influence the work reported in this paper.

References

[1] Paulo E. Arratia, et al., Elastic instabilities of polymer solutions in cross-channel flow, Phys. Rev. Lett. 96 (14) (2006), 144502.
[2] R.J. Poole, M.A. Alves, Paulo J. Oliveira, Purely elastic flow asymmetries, Phys. Rev. Lett. 99 (16) (2007), 164503.
[3] Mahdi Davoodi, Allysson F. Domingues, Robert J. Poole, Control of a purely elastic symmetry-breaking flow instability in cross-slot geometries, J. Fluid Mech. 881 (2019) 1123–1157.
[4] Mahdi Davoodi, et al., Stabilization of purely elastic instabilities in cross-slot geometries, J. Fluid Mech. 922 (2021).

Further reading

[1] M. Davoodi, et al., On the similarities between the simplified Phan-Thien–Tanner model and the finitely extensible nonlinear elastic dumbbell (Peterlin closure) model in simple and complex flows, Phys. Fluids 34 (3) (2022), 033110.